Experimental Study of Synthesis of Heavy Nuclei at JAERI

K. Nishio[1], H. Ikezoe[1], S. Mitsuoka[1], J. Lu[2], K. Satou[1]

1. Advanced Science Research Center, Japan Atomic Energy Research Institute
Tokai-mura, Ibaraki 319-1195, Japan
2. Instiute of Modern Physics, Chinese Academy of Sciences, 730000 Lanzhou, China

Abstract

Evaporation residue (ER) cross sections for ^{82}Se+$^{\rm nat}$Ce and ^{76}Ge+^{150}Nd were measured in the vicinity of the Coulomb barrier, and the fusion probability was obtained with the aid of calculated survival probability. The former system represents fusion of two spherical nuclei, the latter fusion involving the prolately deformed target ^{150}Nd. The collision of ^{76}Ge with the side of ^{150}Nd is more compact in configuration at touching. The system ^{82}Se+$^{\rm nat}$Ce showed fusion hindrance in form of extra-extra-push energy of 27±5 MeV, whereas the system ^{76}Ge+^{150}Nd does not show fusion hindrance at and above the Coulomb barrier energy, suggesting that the reaction starting from the compact touching point results in a higher fusion probability.

1. Introduction

Heavy ion fusion reactions between massive nuclei near the Coulomb barrier have been investigated experimentally and theoretically so far. This is partly because there is a possibility of synthesizing a super-heavy element as an evaporation residue by complete fusion under a proper choice of colliding particles and the bombarding energy. The production of evaporation residues comprises of two separate processes, the fusion process between two interacting nuclei (entrance channel) and the survival process against fission in the course of the deexcitation process (exit channel). The former process is successfully understood by a coupled channel model [1] in the limit of light projectile-target combination of $Z_1Z_2 \leq 1800$. Fusion enhancement relative to the one-dimensional barrier penetration model was observed below the Coulomb barrier region [2]. This could be explained by replacing the one-dimensional barriers by a distribution of barriers [3][4][5]. On the other hand, in heavy systems ($Z_1Z_2 > 1800$), the formation of a compound nucleus is not warranted even if the system overcomes the fusion barrier. This is because at the contact point the distance between the centers of projectile and target is larger than the distance of the centers of the nascent fission fragments at the fission saddle point. The kinetic energy of the interacting nuclei decreases in the course of the fusion process, with the energy being dissipated into the intrinsic excitation energy, and the system fails to surmount the fission saddle point for the bombarding energy corresponding to the Coulomb barrier. To drive the system into the compound nucleus, an additional energy called extra-extra-push energy ($E_{\rm XX}$) is needed.

Collisions that fail to form a compound nucleus may break as quasifission after a significant amount of nucleon transfer and kinetic energy loss. Fission fragments from quasifission are difficult to distinguish experimentally from fission fragments of complete fusion, making the fusion cross section ambiguous when only the fission fragments are measured. Therefore detecting the evaporation residues is essential to identify the fusion reaction and obtain the fusion probability.

There are several investigations on the fusion hindrance of massive system based on the measurement of evaporation residues [5]-[8]. These investigations show that $E_{\rm XX}$ increases with Z_1Z_2 above $Z_1Z_2 \sim 1800$.

We expected that there would be a distinct difference in fusion probability between two types of heavy ion fusions ($Z_1Z_2 > 1800$), one is the fusion of two spherical nculei and the other is the fusion involing largely deformed target, from the consideration that the latter type of fusion has a compact configuration at touching with certain probability.

So, we have measured the ER cross sections of ^{82}Se+$^{\rm nat}$Ce (Z_1Z_2=1972) [10] and ^{76}Ge+^{150}Nd (Z_1Z_2=1920) [9] in order to investigate the effects of nuclear deformation on the entrance channel. $^{\rm nat}$Ce is spherical in shape, whereas ^{150}Nd is largely deformed. From the experimental data, we determied the fusion probability with the help of the survival probability calculated by the statistical model code HIVAP. The parameters describing the deexcitation process in this code was determined so as to reproduce the ER cross section following the fusion of ^{28}Si+^{198}Pt (Z_1Z_2=1092) [9][11].

2. Experiment

Measurement of evaporation residue cross sections following the fusion of ^{82}Se+$^{\rm nat}$Ce and ^{76}Ge+^{150}Nd was made by using ^{82}Se and ^{76}Ge beam supplied by the JAERI-tandem booster accelerator. The targets were made by sputtering the enriched isotopes (Nd_2O_3) or metal ($^{\rm nat}$Ce−metal) on a 1.5 or 0.8 μm thick aluminum foil. Typical target thickness was 400 μg/cm^2. The target was set to a rotating target frame in the target chamber.

Since the evaporation residues produced in the present reaction are α decaying nuclei, the evaporation channels could be identified by observing α-decay energies and life-times. The experimental details are described in elsewhere [11][9], and thus only the essence is written here. The evaporation residues emitted in beam direction were separated in flight from the primary beam by the JAERI recoil mass separater (JAERI-RMS)[12]. The separated recoils were implanted into a double sided position-sensitive strip detector (DPSD). Two large area timing detectors, one positioned in front of the DPSD and the other 30 cm upstream the DPSD, were used to obtain the time-of-flight (TOF) signal of incoming particles. The presence of the TOF signal was used to distinguish ER implantation events from the subsequent α-decays, which generate no TOF signals. A two-dimensional spectrum of the energy versus TOF gave a rough estimate of a mass number of the incoming particle, allowing the distinction of ERs from background particles. Alpha-decay events later than 5 μs after the implantation of ER were recorded. Typical energy resolution of the DPSD was 70 keV(FWHM). A silicon surface barrier detector to monitor the beams was set at 45° direction in the target chamber to determine the absolute values of the ER cross sections.

3. Data analysis and experimental results

The identification for a specific channel was made by counting the ER-α_1-α_2 chains, where ER stands for the events produced when the incoming evaporation residue hits the DPSD. The α_1 and α_2 are the first and the second correlated α-decay event. Figure 1 shows the two-dimensional spectrum of α particle energy and the time interval between the ER implantation and the α decay in the reaction of ^{82}Se+$^{\rm nat}$Ce. All the events shown in Fig.1 satisfy the condition that the position agreement between ER and α event is achieved within (ΔX,ΔY)=(1.0, 1.0) mm. We searched the correlated decay chain, ER-α_1-α_2, to identify the specific evaporation channels with help of the known α decay energy and half-life. The events forming ER-α_1-α_2 chains are shown in Fig.1, where each channel is distinguished by different symbols.

To obtain absolute ER cross sections the efficiency of the ER to be transported to the focal plane detectors through the JAERI-RMS has to be known, which was estimated by the method described in Ref.[9][13]. The estimated transport efficiency for a specific charge state of ER was multiplied by the charge fraction calculated by the Shima formula [14].

The probability of detecting the α decay of evaporation residues implanted in the DPSD was taken into account in the analysis. This is the function of ER kinetic energy (thus the implantation depth) and the α decay energy.

Evaporation residue cross section for ^{76}Ge+^{150}Nd and ^{82}Se+$^{\rm nat}$Ce are shown in Fig.2 and Fig.3 as a function of c.m. energy by solid circles with error bars. The error includes both statistical contributions and the estimated uncertainty of 50% coming from the transport efficiency of ERs through the JAERI-RMS. The ER cross sections for ^{28}Si+^{198}Pt is shown in Fig.4. In this figure we also show the fission cross section (open circle) taken from Ref.[9]. Since the compound nucleus ^{226}U formed by this reaction (^{226}U) is very fissile, the fission cross section is well approximated to the fusion cross section.

4. Discussions

We have calculated the ER cross sections of ^{28}Si+^{198}Pt by using the HIVAP code [15] in order to find the parameters describing the deexcitation process of highly excited neutron deficient uranium isotopes. Details of the parameteris we used in this code can be found in elsewhere [11][9]. The partial wave cross section in the fusion ^{28}Si+^{198}Pt was calculated by the CCDEF code [16]. In this fusion calculation, effects of static deformation of projectile and target in addition to the couplings of inelastic excitations of the projectile and target to the fusion process were taken into account. The calculated fusion cross section shown in Fig.4 nicely reproduces the measured data. The partial wave cross section determined by the CCDEF code was inputted to the HIVAP code as an initial spin distribution and the ER cross section was calculated, which can represent the measured data quite well. For the present heavy systems, ^{76}Ge+^{150}Nd and ^{82}Se+$^{\rm nat}$Ce, the initial spin distribution was again determined by the CCDEF code, and the similar calculaton was made. The results are shown by thick dashed curve (Fig.2;^{76}Ge+^{150}Nd, Fig.3;^{82}Se+$^{\rm nat}$Ce). For ^{76}Ge+^{150}Nd, the calculation predicts the ^{225,224}U channels in $E_{\rm c.m.}$ =185−195 MeV. This is not consistent with the experimental data, where we observed no evaporation residues in this energy region. Above the Coulomb barrer ($V_{\rm B}$ =209MeV), however, the calculation agrees well with the measured data. For the fuiosn ^{82}Se+$^{\rm nat}$Ce, the measred data lies below the calculated cross sections below $E_{\rm c.m.} <230$ MeV, indicating that there is a fusion hindrance up to $E_{\rm c.m.} =1.07V_{\rm B}$ ($V_{\rm B}$ =215.3 MeV for ^{82}Se+^{140}Ce).

The experimental ER cross section $\sigma_{{\rm er},c}$ for the observed channel c was used to obtain the fusion probability weighted by the angular momentum l by

$$P_{\rm fus}(E_{\rm c.m.}) = \frac{\sum_c \sigma_{{\rm er},c}(E_{\rm c.m.})}{\pi\lambda^2 \sum_l (2l+1) \sum_c w_{{\rm er},c}(E_{\rm c.m.}+Q,l)}. \quad (1)$$

The survival probability $w_{{\rm er},c}$ against fission for the specific evaporation channel c is a function of the excitation energy $E_{\rm ex} = E_{\rm c.m.} + Q$ (reaction Q-value) and the angular momentum l. This was calculated by the HIVAP code [15] using present parameters. To check if the present statistical model calculation reasonably provides the survival probability, we have determined the $P_{\rm fus}$ for the fusion reaction ^{28}Si+^{198}Pt, which is the light fusion system with Z_1Z_2=1092 and is expected to have no fusion hindrance. The result is shown in Fig.5 as a function of $E_{\rm c.m.}/V_{\rm B}$, where $V_{\rm B}$=125.5 MeV is the spherical Coulomb barrier for this reaction. Above this barrier $P_{\rm fus}$ is almost constant with 1, indicating that the present HIVAP calculation reasonably reproduces the survival probability.

When fission is the dominant deexcitation channel like in the present case, the evaporation residue cross section does not contain information on the fusion of high partial waves, because they will lead to fission. The surviving l range is limited to $l <\sim 25\hbar$, corresponding to an impact parameter less than 1 fm, and hence P_{fus} is reasonably approximated to that of central collision.

The obtained fusion probability for ^{82}Se+$^{\mathrm{nat}}$Ce is shown in Fig.5 as a function of $E_{\mathrm{c.m.}}/V_{\mathrm{B}}$, where V_{B} is taken as 215.3 MeV of ^{82}Se+^{140}Ce. The error in P_{fus} includes only statistical error. Below $E_{\mathrm{c.m.}}/V_{\mathrm{B}} = 1.15$, P_{fus} for ^{82}Se+$^{\mathrm{nat}}$Ce decreases considerably with lowering the bombarding energy, exhibiting the curve similar to the massive system having fusion hindrance [5][7][8]. By finding the $E_{\mathrm{c.m.}}$ at which P_{fus} of ^{82}Se+$^{\mathrm{nat}}$Ce crosses the P_{fus}=0.5 level, we obtained the extra-extra-push energy E_{XX}=27±5 MeV for this reaction.

The fusion probability P_{fus} for ^{76}Ge+^{150}Nd is shown in Fig.5 by the solid circles with statistical error bars. P_{fus}-values of ^{76}Ge+^{150}Nd is nearly flat with ∼1.0 down to $E_{\mathrm{c.m.}} \sim V_{\mathrm{B}}$. ($V_{\mathrm{B}}$=209.0 MeV). This trend is similar to the fusion of ^{28}Si+^{198}Pt which exhibits no fusion hindrance, and the spectrum shows marked contrast to that of ^{82}Se+$^{\mathrm{nat}}$Ce. It is apparent that the reaction ^{76}Ge+^{150}Nd has no fusion hindrance above the spherical Coulomb barrier. We did not observe any event in $E_{\mathrm{c.m.}} < V_{\mathrm{B}}$ and thus the upper limit is shown by the solid reversed-triangle in Fig.5.

Fusion probability can be represented by assuming the fusion barrier distribution to have Gaussian in shape [7][8]. By adjusting the center of the barrier and the standard deviation, we could represent the P_{fus} for ^{82}Se+$^{\mathrm{nat}}$Ce as shown in Fig.5 (solid curve). The corresponding partial wave cross section was calculated and inputted to the HIVAP code as an initial spin distribution, and the ER cross section was calculated. This is shown in Fig.3 (solid curve), which reproduces the experimetal ER cross sections quite well.

We tried to reproduce the ER cross section for ^{76}Ge+^{150}Nd by assuming the extra-extra-push energy (E_{XX}) to depend on the colliding angle θ_{coll} of ^{76}Ge on the central axis of ^{150}Nd,

$$E_{\mathrm{XX}}(r) = E_{\mathrm{XX0}} \frac{r - R_{\mathrm{side}}}{R_{\mathrm{tip}} - R_{\mathrm{side}}}, \tag{2}$$

and the Coulomb barrier height was raised to an amount, E_{XX}, from the original barrier of the CCDEF code. Here, the Coulomb barrier distance r is a function of θ_{coll}. R_{side} (=11.7 fm) and R_{tip} (=14.6 fm) are the distance of side collision and that of tip collision, respectively, for ^{76}Ge+^{150}Nd. When E_{XX0} is taken to be 13 MeV, the ^{224,225}U cross sections are suppressed (solid curve in Fig.2), which becomes consistent with the experimental data. It is noted that we assume no fusion hindrance for the side collision in Eq.(2), meaning that the side collision exhibits larger fusion probability than the fusion starting from the distant touching point.

5. Conclusions

Evaporation residue cross sections for ^{76}Ge+^{150}Nd and ^{82}Se+$^{\mathrm{nat}}$Ce were measured in the vicinity of the Coulomb barrier. The fusion of ^{82}Se+$^{\mathrm{nat}}$Ce is a rection characterized by the spherical and massive colliding partners with $Z_1 Z_2$ =1972, and fusion hindrance was observed in the form of the extra-extra-push energy of 27±5 MeV. For the reaction ^{76}Ge+^{150}Nd, which has a $Z_1 Z_2$ value of 1920 close to ^{82}Se+$^{\mathrm{nat}}$Ce, the obtained fusion probability formed striking contrasts to the fusion of ^{82}Se+$^{\mathrm{nat}}$Ce and does not exhibit fusion hindrance at all above the spherical Coulomb barrier. The ER cross section was reproduced when the extra-extra-push energy is assumed only on the tip collision in ^{76}Ge+^{150}Nd. The enhanced fusion probability at the Coulomb barrier for the ^{76}Ge+^{150}Nd reaction compared to the ^{82}Se+$^{\rm nat}$Ce, as well as the no fusion hindrance for the side collidion in ^{76}Ge+^{150}Nd suggests that the reaction starting from the compact touching point results in higher fusion probability than the fusion from the distant touching point.

References

[1] A.B. Balantekin and N. Takigawa, Rev. Mod. Phys. **70**, 77 (1998).

[2] M. Dasgupta, D.J. Hinde, N. Rowley, and A.M. Stefanini, Annu. Rev. Nucl. Part. Sci. **48**, 401 (1998).

[3] N. Rowley, G.R. Satchler, and P.H. Stelson, Phys. Lett. B **254**, 25 (1991).

[4] W. Reisdorf, F.P. Hessberger, K. D. Hildenbrand, S. Hofmann, G. Münzenberg, K.-H. Schmidt, J.H.R. Schneider, W.F.W. Schneider, K. Sümmerer, G. Wirth, J.V. Kratz, and K. Schlitt, Phys. Rev. Lett. **49**, 1811 (1982).

[5] J.G. Keller, K.-H. Schmidt, F.P. Hessberger, G. Münzenberg, W. Reisdorf, H.-G. Clerc, and C.-C. Sahm, Nucl. Phys. **A452**, 173 (1986).

[6] C.-C. Sahm, H.-G. Clerc, K.-H. Schmidt, W. Reisdorf, P. Armbruster, F.P. Hessberger, J.G. Keller, G. Münzenberg, and D. Vermeulen, Z. Phys. A, **319**, 113 (1984).

[7] C.-C. Sahm, H.-G. Clerc, K.-H. Schmidt, W. Reisdorf, P. Armbruster, F.P. Hessberger, J.G. Keller, G. Münzenberg, and D. Vermeulen, Nucl. Phys. **A441**, 316 (1985).

[8] A.B. Quint, W. Reisdorf, K.-H. Schmidt, P. Armbruster, F.P. Hessberger, S. Hofmann, J. Keller, G. Münzenberg, H. Stelzer, H.-G. Clerc, W. Morawek, C.-C. Sahm, Z. Phys. A **346**, 119 (1993).

[9] K. Nishio, H.Ikezoe, S. Mitsuoka, and J. Lu, Phys. Rev. C, **62**, 014602 (2000).

[10] K. Nishio, H.Ikezoe, S. Mitsuoka, and K. Satou, S.C. Jeong Phys. Rev. C, submitted.

[11] S. Mitsuoka, H. Ikezoe, K. Nishio and J. Lu, Phys. Rev. C, **62** 054603 (2000).

[12] H. Ikezoe, Y. Nagame, T. Ikuta, S. Hamada, I. Nishinaka and T. Ohtsuki, Nucl. Instrum. Meth. A **376**, 420 (1996)

[13] T. Kuzumaki, H. Ikezoe, S. Mitsuoka, T. Ikuta, S. Hamada, Y. Nagame, I. Nishinaka, O. Hashimoto, Nucl. Instrum. Meth. A, **437**, 107 (1999)

[14] K. Shima, T. Ishihara and T. Mikuno, Nucl. Instrum. Meth. **200**, 605 (1982)

[15] W. Reisdorf and M. Schädel, Z. Phys. A **343**, 47 (1992).

[16] J.O. Fernández Niello, C.H. Dasso and S. Landowne, Comput. Phys. Commun. **54**, 409 (1989).

Fig.1 Events of ER-α correlation plotted on the plane of α energy (E_α) and time interval (τ) for $^{82}\mathrm{Se}+^{\mathrm{nat}}\mathrm{Ce}$ ($E_{\mathrm{c.m.}} = 245.0$ MeV). Each box represents α decay character having ±60 keV energy width around the known α line and time interval of $\frac{1}{10}T_{\frac{1}{2}} < \tau < 10T_{\frac{1}{2}}$. Correlated chain ER-α_1-α_2 is shown depending on the channel.

Fig.2 Evaporation residue cross sections for $^{76}\mathrm{Ge}+^{150}\mathrm{Nd}$ as a function of c.m. energy. Excitation energy of the compound nucleus, E_{ex}, is also indicated. In (a) and (h), the upper limit of the ER cross section is indicated (reverseed triangle). Dashed curve is the results of the statistical model calculation (HIVAP code) coupled with the CCDEF code. We obtain the solid curves when extra-extra-push energy of eq.(2) is considered in the fusion barrier height.

Fig.3 ER cross sections for ^{82}Se+$^{\mathrm{nat}}$Ce. The lower right section is the sum of the cross sections over the channels (a)-(g). Reversed triangle is the upper limit. Dashed curve is the HIVAP calculation with the partial wave cross section determined by the coupled channel calculation. When the Gaussian shape fusion barrier distribution with E_{XX} =27 MeV is adopted in the fusion process, one obtains the solid curve.

Fig.4 Fusion (open) and evaporation residue (solid) cross sections for ^{28}Si+^{198}Pt. Thick solid curve is the results of the statistical model calculation (HIVAP code) coupled with the CCDEF code. For (a) $\sim$ (f), the cross section includes the components noted in each portion of the figure, and the calculated cross sections of the constituent are show by the dash-dotted (uranium), dotted (thorium or protactinium) and dashed (radium or actinium) curves. The fusion cross section based on the coupled channels calculation is shown by thin solid curve, and the one-dimensional barrier penetration model gives thin dash-dot-dotted curve.

Fig.5 Fusion probability determined from the experimental ER cross sections.

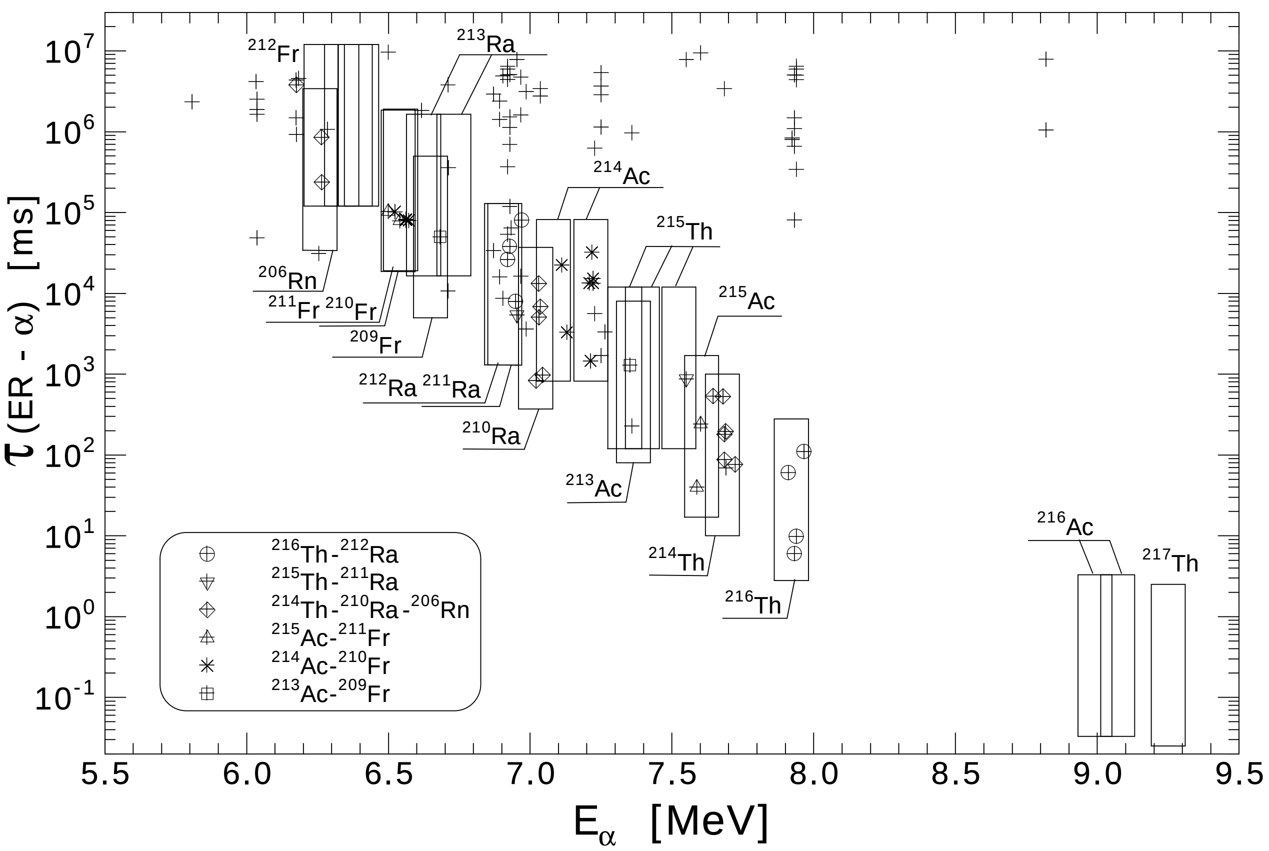

τ (ER - α) [ms]
E_α [MeV]
10^7
10^6
10^5
10^4
10^3
10^2
10^1
10^0
10^{-1}
5.5
6.0
6.5
7.0
7.5
8.0
8.5
9.0
9.5
^{212}Fr
^{213}Ra
^{214}Ac
^{215}Th
^{215}Ac
^{206}Rn
^{211}Fr
^{210}Fr
^{209}Fr
^{212}Ra
^{211}Ra
^{210}Ra
^{213}Ac
^{214}Th
^{216}Th
^{216}Ac
^{217}Th
^{216}Th-^{212}Ra
^{215}Th-^{211}Ra
^{214}Th-^{210}Ra-^{206}Rn
^{215}Ac-^{211}Fr
^{214}Ac-^{210}Fr
^{213}Ac-^{209}Fr

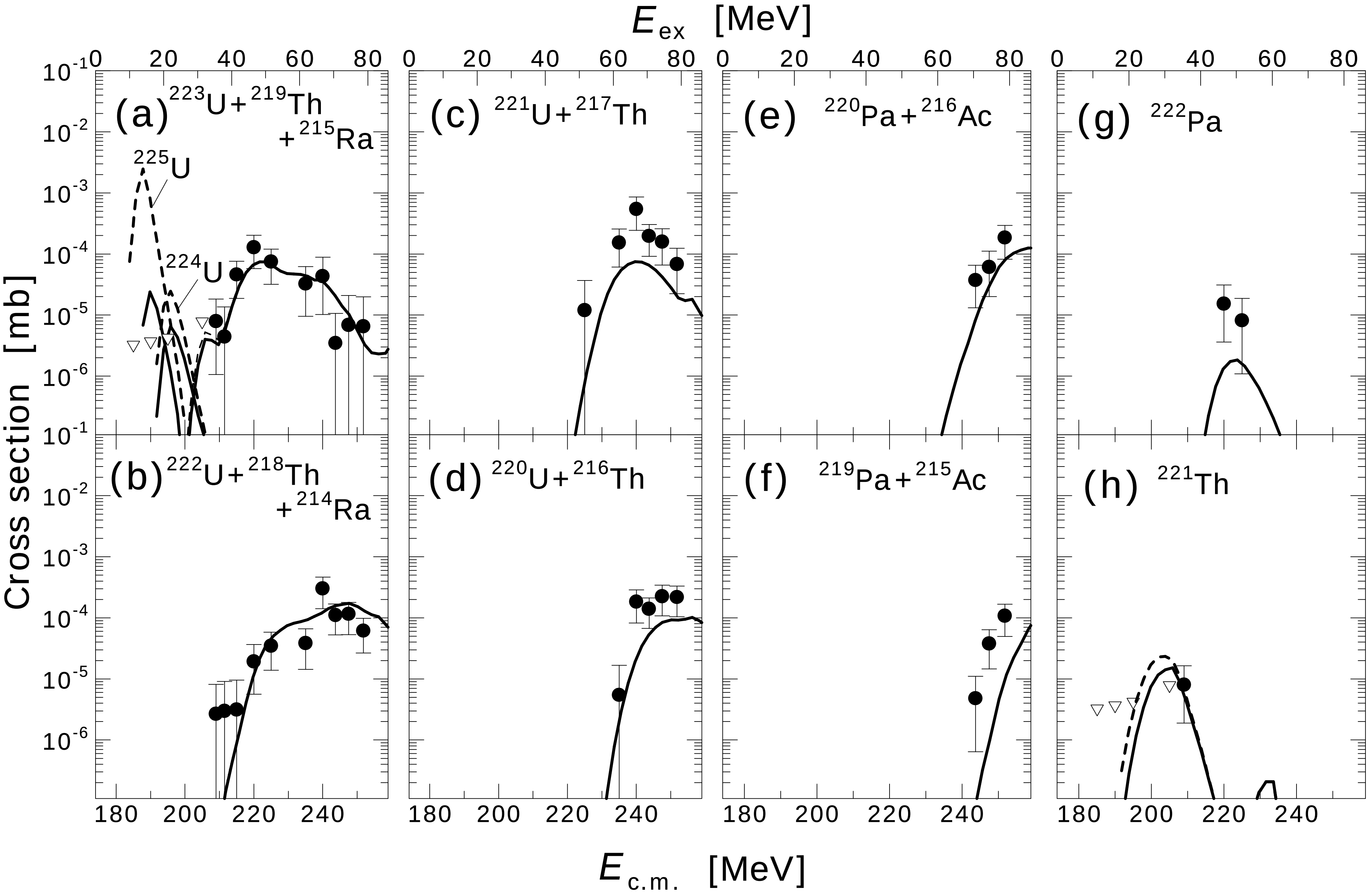E_{ex} [MeV]
0
20
40
60
80
Cross section [mb]
10^{-1}
10^{-2}
10^{-3}
10^{-4}
10^{-5}
10^{-6}
(a) ^{223}U+^{219}Th +^{215}Ra
^{225}U
^{224}U
(b) ^{222}U+^{218}Th +^{214}Ra
(c) ^{221}U+^{217}Th
(d) ^{220}U+^{216}Th
(e) ^{220}Pa+^{216}Ac
(f) ^{219}Pa+^{215}Ac
(g) ^{222}Pa
(h) ^{221}Th
180
200
220
240
$E_{\mathrm{c.m.}}$ [MeV]

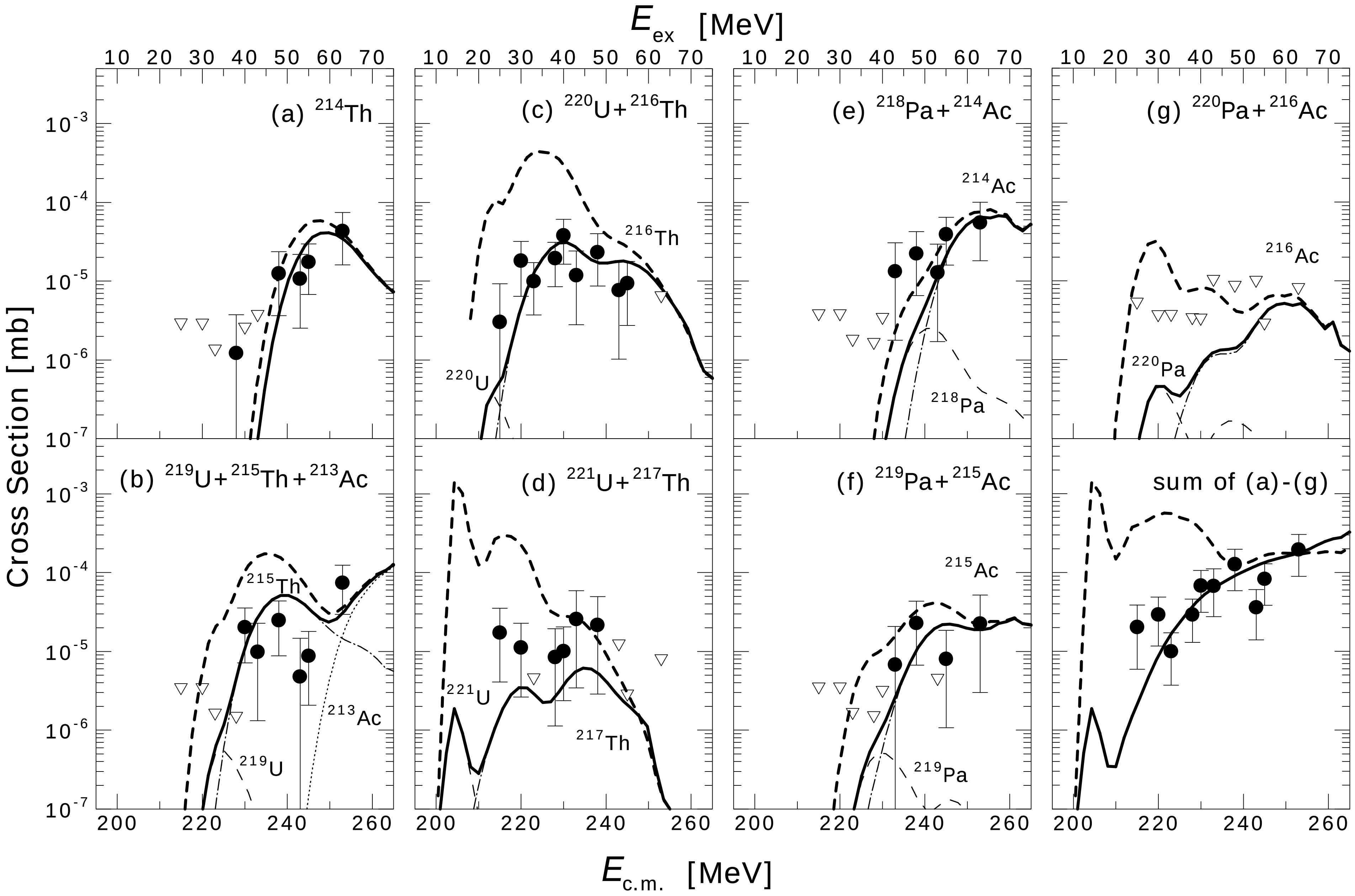
E_{ex} [MeV]
10 20 30 40 50 60 70
Cross Section [mb]
10^{-3}
10^{-4}
10^{-5}
10^{-6}
10^{-7}
(a) ^{214}Th
(b) ^{219}U+^{215}Th+^{213}Ac
^{215}Th
^{213}Ac
^{219}U
(c) ^{220}U+^{216}Th
^{216}Th
^{220}U
(d) ^{221}U+^{217}Th
^{221}U
^{217}Th
(e) ^{218}Pa+^{214}Ac
^{214}Ac
^{218}Pa
(f) ^{219}Pa+^{215}Ac
^{215}Ac
^{219}Pa
(g) ^{220}Pa+^{216}Ac
^{216}Ac
^{220}Pa
sum of (a)-(g)
200 220 240 260
$E_{c.m.}$ [MeV]

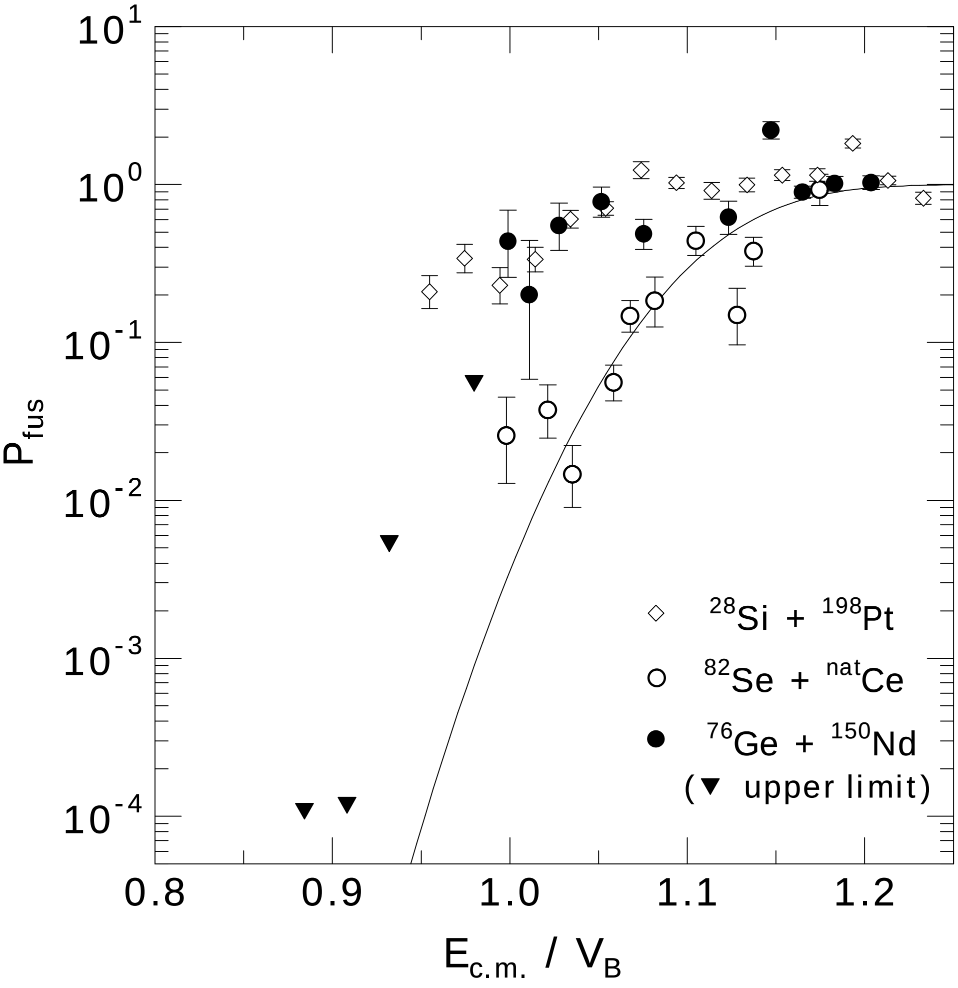
10^1
10^0
10^{-1}
10^{-2}
10^{-3}
10^{-4}
P_{fus}
0.8
0.9
1.0
1.1
1.2
$E_{c.m.} / V_B$
◇ ^{28}Si + ^{198}Pt
○ ^{82}Se + ^{nat}Ce
● ^{76}Ge + ^{150}Nd
(▼ upper limit)